BIOCHEMISTRY
including biophysical chemistry & molecular biology
Article

Biochemistry **2010,** *49,* 4339–4348 4339
DOI: 10.1021/bi9020583

pH-Mediated Fluorescence and G-Quadruplex Binding of Amido Phthalocyanines[†]

Jawad Alzeer and Nathan W. Luedtke*

Institute of Organic Chemistry, University of Zürich, Winterthurerstrasse 190, Switzerland 8057

Received December 2, 2009; Revised Manuscript Received April 8, 2010

ABSTRACT: A new family of G-quadruplex ligands termed "amido phthalocyanines" (APcs) was synthesized by reacting variable amino acids with tetraamino zinc phthalocyanine. Variation in the number of methylene units separating the APc scaffold from terminal ammonium groups systematically modulated ammonium pK_a values that, in turn, mediated APc aggregation and DNA binding. Certain APcs exhibited nearly 1000-fold enhancements in fluorescence quantum yield upon binding G-quadruplex DNA under physiological conditions of pH and ionic strength. G-quadruplexes derived from the c-myc and c-kit promoters and the human telomeric repeat were evaluated for APc affinity and specificity using two complementary and direct fluorescence binding assays that revealed apparent dissociation constants ranging from 20 to 200 nM. Approximately 500-fold lower affinities for duplex and single-stranded DNAs were observed. Interestingly, APc−quadruplex binding was relatively insensitive to ionic strength (0.03−1 M KCl) but highly dependent on the pH of the solution. Our results provide a mechanism for the "turn-on" fluorescence properties exhibited by these compounds that will assist in future rational design of new G-quadruplex-specific fluorescent probes and drug candidates.

Molecular recognition of specific DNA sequences is fundamental to the control of gene expression and can provide important new opportunities for therapeutic intervention (*1*−*3*). Sequence-specific targeting of DNA in the context of the human genome typically requires molecules that can span 10 or more base pairs of duplex DNA (*4*). Antisense oligonucleotides and polyamide-based derivatives can exhibit outstanding sequence specificity and affinity but are often too large and charged to exhibit good cellular uptake and pharmacokinetics (*5*, *6*). Many clinically important chemotherapeutic agents are small molecules (e.g., cisplatin, mitomycin C, and daunomycin) that bind DNA nonspecifically and cause a wide variety of side effects including secondary cancer formation. Small molecules that specifically bind to particular DNA secondary structures might exhibit improved cancer-specific targeting and decreased side effects. G-quadruplexes are highly attractive receptors for the rational design of small molecules given the abundant information available regarding their structures (*7*−*10*), thermodynamic stabilities (*11*), and potential biological activities, some of which have been implicated in cancer growth (*12*, *13*). Given the vast number of potential G-quadruplex-forming sequences in prokaryotic and eukaryotic genomes (*14*−*18*), it is essential that basic principles for G-quadruplex−small molecule binding are established so that highly selective recognition can be achieved.

A wide variety of scaffolds for targeting G-quadruplexes have recently been reported (*19*−*30*). Polycyclic compounds with large, planar surfaces can bind G-quadruplexes through end-stacking interactions onto one or both terminal G-tetrads (*7*, *8*, *23*−*25*). According to computational modeling, phthalocyanines have especially good shape complementarity with the stacked G-tetrads that constitute G-quadruplex DNA (Figure 1). Variable cationic groups like guanidinium (*26*), pyridinium (*27*), and tertiary ammonium (*28*, *29*) incorporated onto phthalocyanine and porphyrazine scaffolds can provide water-soluble derivatives with excellent G-quadruplex affinity and specificity. While electrostatic interactions have been implicated as important factors in driving these interactions (*30*), nothing is known about how the spacing between cationic groups and the phthalocyanine scaffold might affect G-quadruplex affinity and specificity. We therefore prepared a new family of derivatives termed amido phthalocyanines (APcs)[1] where systematic variation of methylene units separating ammonium groups from the phthalocyanine scaffold might optimize the distances for electrostatic/hydrogen-bonding interactions with the phosphodiester backbone (Figure 1). APcs were synthesized by reacting tetraamino zinc phthalocyanine (**1**) with the N-Boc-protected symmetric anhydrides of glycine, β-alanine, γ-aminobutyric acid, and δ-aminovaleric acid. Boc deprotection furnished compounds **2**−**5** in total isolated yields ranging from 50% to 87%. Subsequent biophysical analysis of the G-quadruplex binding affinity and specificity revealed that the variable number of methylene units in these compounds modulates the pK_a values of their ammonium groups that, in turn, influence phthalocyanine aggregation and DNA binding. These results provide a mechanism for the "turn-on" fluorescence properties of phthalocyanines that should facilitate

[†]Supported by the Swiss National Science Foundation (116868 to N.W.L.), the Dr. Helmut Legerlotz Stiftung (J.A.), and the University of Zürich (OCI).

*To whom correspondence should be addressed. Telephone: +41 44 635 4244. Fax: +41 44 635 6891. E-mail: luedtke@oci.uzh.ch.

[1]Abbreviations: APc, amido phthalocyanine; Boc, *tert*-butyloxycarbonyl; CD, circular dichroism; CT DNA, calf thymus DNA; DMAP, *N*, *N*-dimethylaminopyridine; DCC, dicyclohexylcarbodiimide; DMF, dimethylformamide; DMSO, dimethyl sulfoxide; EC_{50}, half-maximal effective concentration; EDTA, ethylenediaminetetraacetic acid; HF, Hartree−Fock; MALDI TOF MS, matrix-assisted laser desorption/ionization time-of-flight mass spectrometry; NMR, nuclear magnetic resonance; TFA, trifluoroacetic acid; THF, tetrahydrofuran; TKE, Tris−potassium−EDTA buffer; $tRNA^{mix}$, mixture of pretransfer and mature transfer ribonucleic acids.

Published on Web 04/09/2010

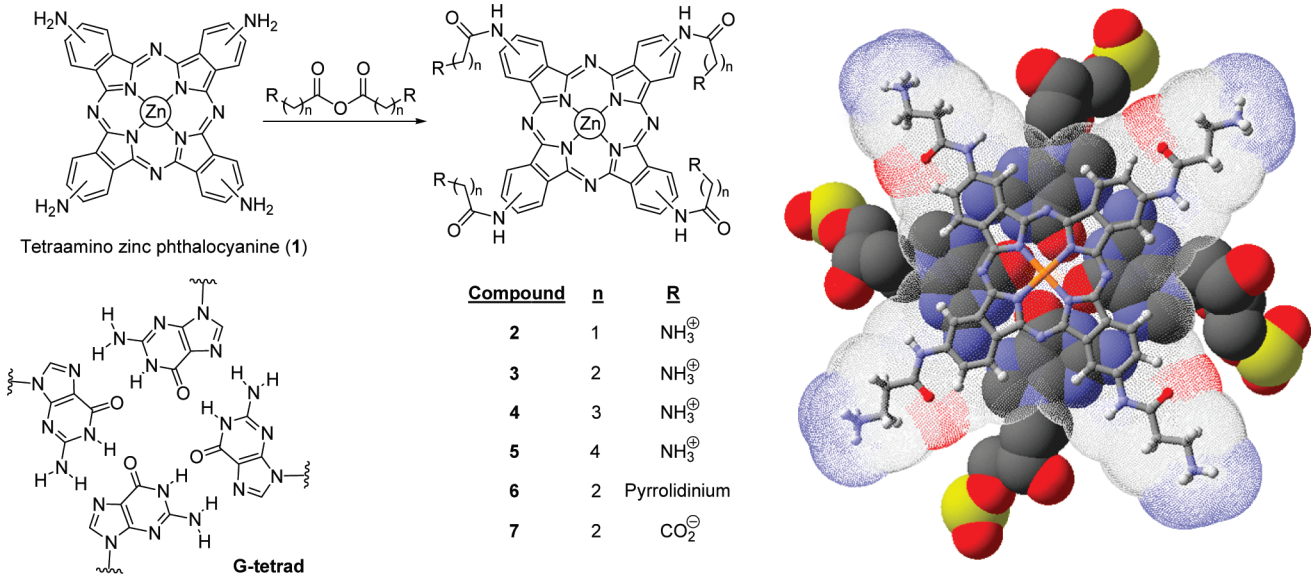

FIGURE 1: Synthesis and structures of amido phthalocyanines (**2**−**7**) as compared to G-tetrad DNA. A theoretical model for phthalocyanine−tetrad stacking was made by using HF/STO-3G to calculate a geometry-optimized C_{4h} symmetric model of compound **3** that was manually docked onto the known coordinates of a terminal G-tetrad from the crystal structure of the parallel human telomeric quadruplex (space-filling model, 1KF1) (*38*). A solvent-accessible surface of 1.4 Å was added to compound **3** using Swiss-PdbViewer 3.7. Similar modeling results are expected for the c-myc and c-kit2 quadruplexes as they can also adopt parallel structures in solution (*48*, *51*).

future design efforts toward optimized fluorescent probes and drug candidates.

MATERIALS AND METHODS

Tetraamino zinc phthalocayanine (**1**) was synthesized and purified as described (*31*, *32*). Pyridine, dicyclohexylcarbodiimide (DCC), N-Boc-protected amino acids, and *N*,*N*-dimethylamino-pyridine (DMAP) were purchased from Fluka. All other reagents were obtained in the highest commercially available grades from Sigma Aldrich. ^{1}H NMR spectra were measured using a Bruker AV-400 spectrometer. Chemical shifts are given in parts per million relative to the residual signal from DMSO-d_6 (δ = 2.50 ppm). For matrix-assisted laser desorption/ionization (MALDI) measurements, α-cyano-4-hydroxycinamic acid and a Bruker Autoflex were used. Precipitates during APc purification were collected using an Eppendorf 5804 centrifuge (7000 rpm) and 50 mL polypropylene tubes. Absorbance and fluorescence were measured using a SpectraMax MP5 spectrophotometer. High clarity, color-free 1.7 mL polypropylene tubes from Axygen were used for making serial dilutions and CD samples. Binding assays were conducted in Corning 384-well black polystyrene assay plates with nonbinding surfaces (final reaction volumes = 70 μL). All binding reactions were conducted at room temperature in a "TKE" buffer containing 50 mM Tris-HCl, 150 mM KCl, and 0.5 mM EDTA (pH 7.4 unless indicated otherwise). APc stock solutions were prepared at 2 mM in deionized water and diluted into TKE buffer immediately before use.

Tetrakis(*2-aminoacetamido*) *Zinc Phthalocyanine·TFA*$_4$ (***2***). DCC (453 mg, 2.2 mmol) was added to a solution of N-Boc-Gly-OH (700 mg, 4 mmol) in THF (5 mL) at room temperature and under dry N_2. After 2 h, white precipitate was removed and the filtrate evaporated and dried under high vacuum to afford 660 mg (2 mmol) of the crude symmetric anhydride. This material was dissolved in pyridine (4 mL) containing tetraamino zinc phthalocyanine **1** (50 mg, 0.078 mmol) and DMAP (244 mg, 2 mmol). The mixture was stirred under dry N_2 at 70 °C. After 3 days, the reaction was cooled to room temperature and diluted with ether (40 mL) and the precipitate collected by centrifugation. This material was repeatedly washed with ether and EtOAc, dried, and carried directly over into the next step. Boc groups were removed at room temperature using TFA (3 mL) in CH_2Cl_2 (15 mL). After 4 h, the resulting precipitate was collected by centrifugation, repeatedly washed with CH_2Cl_2, and dried to afford **2** (83 mg, 80%, over two steps) as a dark green solid. ^{1}H NMR (300 MHz, DMSO-d_6) δ 11.29 (br s, 4H), 9.79 (br d, 4H), 9.37 (m, 4H), 8.39 (br s, 4(NH_3)), 8.36 (m, 4H), 4.09 (br s, 8H). MALDI TOF MS (*m*/*z*) $[M + H]^+$ calcd for $C_{40}H_{32}N_{16}O_4Zn$, 865.2; found, 865.2. HR ESI MS $[M + 2H]^{2+}$ calcd for $C_{40}H_{32}N_{16}O_4Zn$, 433.1115; found, 433.1110. UV−vis (DMSO) λ_{max} (nm) and ε (cm^{-1} M^{-1}) 360 (6.97×10^4), 630 (2.82×10^4), and 690 (1.58×10^5).

Tetrakis(*3-aminopropanamido*) *Zinc Phthalocyanine·TFA*$_4$ (***3***). DCC (240 mg, 1.16 mmol) was added to a solution of Boc-β-alanine-OH (400 mg, 2.1 mmol) in THF (5 mL) at room temperature and under dry N_2. After 2 h, white precipitate was removed and the filtrate evaporated and dried to afford 380 mg (1.05 mmol) of the crude symmetric anhydride that was dissolved in DMF (3 mL) containing tetraamino zinc phthalocyanine **1** (50 mg, 0.078 mmol) and *N*-methylmorpholine (179 μL, 1.63 mmol). After being stirred for 2 days at 60 °C, DMF was removed under reduced pressure. The resulting precipitate was repeatedly washed with ether/hexane (1:1) and MeOH/ether/hexane (0.1:1:1), dried, and carried directly over into the next step. Boc groups were removed at room temperature with TFA (1 mL). After 2 h, the reaction mixture was diluted with EtOAc (9 mL), and the resulting precipitate was collected by centrifugation. The precipitate was repeatedly washed with EtOAc and dried to afford **3** (53 mg, 87%) as a dark green solid. ^{1}H NMR (300 MHz, DMSO-d_6) δ 11.05 (br s, 4H), 9.85 (br s, 4H), 9.31 (m, 4H), 8.35 (m, 4H), 8.03 (br s, 4(NH_3)), 3.34 (br s, 8H), 3.02 (br s, 8H). MALDI TOF MS (*m*/*z*) $[M + H]^+$ calcd for $C_{44}H_{40}N_{16}O_4Zn$, 921.3; found, 921.3. HR ESI MS $[M + 2H]^{2+}$ calcd for $C_{44}H_{40}N_{16}O_4Zn$, 461.1428; found, 461.1425. UV−vis (DMSO) λ_{max} (nm) and ε (cm^{-1} M^{-1}) 360 (6.7×10^4), 630 (3.14×10^4), and 690 (1.54×10^5).

Tetrakis(4-aminobutanamido) Zinc Phthalocyanine·TFA$_4$ (**4**). DCC (185 mg, 0.89 mmol) was added to a solution of N-Boc-γ-aminobutyric acid-OH (331 mg, 1.63 mmol) in THF (5 mL) at room temperature under dry N_2. After 2 h, white precipitate was removed and the filtrate evaporated and dried to afford 310 mg (0.8 mmol) of the crude symmetric anhydride that was dissolved into DMF (4 mL) containing tetraamino zinc phthalocyanine **1** (50 mg, 0.078 mmol) and *N*-methylmorpholine (179 μL, 1.63 mmol). After 7 days at room temperature, DMF was removed under reduced pressure, and the resulting precipitate was repeatedly washed with ether/hexane (3:1) and MeOH/ether/hexane (0.1:1:1), dried, and carried directly over into the next step. Boc groups were removed at room temperature with TFA (1 mL). After 2 h, the reaction mixture was diluted with EtOAc/hexane (9 mL, 3:1), and the resulting precipitate was collected by centrifugation. The precipitate was repeatedly washed with EtOAc/MeOH (20:1) and dried to afford **4** (33 mg, 50%) as a dark green solid. ^{1}H NMR (300 MHz, DMSO-d_6) δ 10.89 (br s, 4H), 9.89 (br s, 4H), 9.31 (m, 4H), 8.36 (m, 4H), 7.92 (br s, 4(NH_3)), 3.05 (br s, 8H), 2.72 (br s, 8H), 2.13 (br s, 8H). MALDI TOF MS (*m*/*z*) $[M + 2H]^{1+}$ calcd for $C_{48}H_{48}N_{16}O_4Zn$, 978.3; found, 978.4. HR ESI MS $[M + 2H]^{2+}$ calcd for $C_{48}H_{48}N_{16}O_4Zn$, 489.1741; found, 489.1738. UV−vis (DMSO) λ_{max} (nm) and ε (cm^{-1} M^{-1}) 360 (6.5×10^4), 630 (3.08×10^4), and 690 (1.43×10^5).

Tetrakis(5-aminopentanamido) Zinc Phthalocyanine·TFA$_4$ (**5**). DCC (175 mg, 0.84 mmol) was added to a solution of N-Boc-δ-aminovaleric acid-OH (335 mg, 1.54 mmol) in THF (4 mL) at room temperature under dry N_2. After 2 h, white precipitate was removed and the filtrate evaporated and dried to afford 330 mg (0.77 mmol) of the crude symmetric anhydride that was dissolved into DMF (4 mL) containing tetraamino zinc phthalocyanine **1** (50 mg, 0.078 mmol) and *N*-methylmorpholine (169 μL, 1.54 mmol). After 7 days at room temperature, DMF was removed under reduced pressure, and the resulting precipitate was repeatedly washed with ether, MeOH/ether/hexane (0.1:1:1), and EtOAc, then dried, and carried directly over into the next step. Boc groups were removed at room temperature with TFA (1 mL). After 2 h, the reaction mixture was diluted with EtOAc/hexane (9 mL, 3:1), and the resulting precipitate was collected by centrifugation. The precipitate was repeatedly washed with EtOAc/MeOH (20:1) and dried to afford **5** (59 mg, 72%) as a dark green solid. ^{1}H NMR (300 MHz, DMSO-d_6) δ 10.87 (br s, 4H), 9.85 (d, 4H), 9.25 (m, 4H), 8.37 (m, 4H), 7.89 (br s, 4(NH_3)), 2.97 (br s, 8H), 2.70 (br s, 8H), 1.89 (br s, 8H), 1.81 (br s, 8H). MALDI TOF MS (*m*/*z*) $[M + 2H]^{1+}$ calcd for $C_{52}H_{56}N_{16}O_4Zn$, 1034.4; found, 1034.4. HR ESI MS (*m*/*z*) $[M + H]^{2+}$ calcd for $C_{52}H_{56}N_{16}O_4Zn$, 517.2054; found, 517.2050. UV−vis (DMSO) λ_{max} (nm) and ε (cm^{-1} M^{-1}) 360 (6.8×10^4), 630 (2.95×10^4), and 690 (1.56×10^5).

Tetrakis[3-(pyrrolidin-1-yl)propanamido] Zinc Phthalocyanine (**6**). DCC (198 mg, 0.99 mmol) was added to a solution of 3-pyrrolidine-1-propionic acid (313 mg, 1.8 mmol) in THF (6 mL) at room temperature and under dry N_2. After 2 h, white precipitate was removed and the filtrate evaporated and dried to afford 330 mg (0.97 mmol) of the crude symmetric anhydride that was dissolved into DMF (3 mL) containing tetraamino zinc phthalocyanine **1** (50 mg, 0.078 mmol) and *N*-methylmorpholine (169 μL, 1.54 mmol). After 7 days at 50 °C, DMF was removed under reduced pressure, and the resulting precipitate was repeatedly washed with ether and MeOH/ether (1:1) and dried to afford **6** (46 mg, 51%) as a dark green solid. ^{1}H NMR (300 MHz, DMSO-d_6) δ 11.17 (br s, 4H), 10.60 (br s, 4H), 9.70 (br s, 4H), 9.25 (br s, 4H), 3.28 (br s, 16H), 2.14 (br s, 8H), 1.97 (br s, 8H). MALDI TOF MS (*m*/*z*) $[M + H]^+$ calcd for $C_{60}H_{64}N_{16}O_4Zn$, 1137.5; found, 1137.5. HR ESI MS (*m*/*z*) $[M + H]^{2+}$ calcd for $C_{60}H_{64}N_{16}O_4Zn$, 569.2367; found, 569.2364. UV−vis (DMSO) λ_{max} (nm) and ε (cm^{-1} M^{-1}) 360 (6.58×10^4), 630 (2.84×10^4), and 690 (1.46×10^5).

Tetrakis(succinate) Zinc Phthalocyanine·Na$_4$ (**7**). Succinic anhydride (196 mg, 1.96 mmol) and DMAP (138 mg, 0.3 mmol) were added to a solution of tetraamino zinc phthalocyanine (50 mg, 0.078 mmol) in DMF (6 mL) at room temperature and under dry N_2. After 7 days, the reaction mixture was diluted with EtOAc (66 mL), and the resulting precipitate was collected by centrifugation. The dark green precipitate was washed repeatedly with H_2O, dried, dissolved into TFA (4 mL), mixed with water (20 mL), and centrifuged. The resulting precipitate was dissolved into 1 N NaOH (50 mL) and MeOH (100 mL) added. The resulting precipitate was dried to afford **4** (76 mg, 86%) as a dark green solid. ^{1}H NMR (300 MHz, DMSO-d_6) δ 8.93 (br s, 4H), 8.13 (br m, 4H), 8.01 (br s, 4H), 6.66 (br m, 4H), 2.92 (br s, 8H), 2.81 (br s, 8H). MALDI TOF MS (*m*/*z*) $[M + H]^+$ calcd for $C_{48}H_{36}N_{12}O_{12}Zn$, 1037.2; found, 1037.2. HR ESI MS (*m*/*z*) $[M - 2H]^{-2}$ calcd for $C_{48}H_{36}N_{12}O_{12}Zn$, 517.0850; found, 517.0864. UV−vis (DMSO) λ_{max} (nm) and ε (cm^{-1} M^{-1}) 360 (6.1×10^4), 630 (2.57×10^4), and 690 (1.32×10^5).

Nucleic Acids. Oligonucleotide DNAs were purchased as HPLC-purified products from Sigma-Genosys. Oligonucleotide solutions (~30 μM) were prepared by mixing the dried oligonucleotides with a "TKE" buffer containing 50 mM Tris-HCl (pH 7.4), 150 mM KCl, and 0.5 mM EDTA. The solutions were heated to 95 °C for 3 min and then slowly cooled to room temperature (over approximately 3 h) before use. Oligonucleotide names, sequences, and extinction coefficients (260 nm) used for estimating stock solution concentrations (in pure water) were as follows: "Htelo", GTTA$(GGGTTA)_4$GG, 306900 cm^{-1} M^{-1}; "Htelo-mut", GTTA$(GAGTTA)_4$GG, 319300 cm^{-1} M^{-1}; "Htelo-C", CC$(TAACCC)_4$TAAC, 274000 cm^{-1} M^{-1}; "F1-Htelo", fluorescein-GTTA$(GGGTTA)_4$GG, 341900 cm^{-1} M^{-1}; "F1-Htelo-mut", fluorescein-GTTA$(GAGTTA)_4$GG, 354300 cm^{-1} M^{-1}; "c-kit2", $(C)_3GGGC(G)_3CGCGA(G)_3A(G)_4AGG$, 253400 cm^{-1} M^{-1}; "Fl-c-kit2", fluorescein-$(C)_3GGGC(G)_3CGCGA(G)_3A(G)_4AGG$, 288400 cm^{-1} M^{-1}; "Fl-c-myc", fluorescein-$(G)_4A(G)_3T(G)_4A(G)_3T(G)_4AA(G)_2T(G)_4$, 356500 cm^{-1} M^{-1}. tRNA Sigma Type X-SA was dissolved into TKE at room temperature and quantified using ε = 9640 cm^{-1} M^{-1} ntd^{-1} (25 °C). Type I, highly polymerized calf thymus DNA was dissolved into TKE at 37 °C overnight (12 h) and centrifuged at 20000*g* and the supernatant diluted by 2-fold into TKE buffer. The CT DNA solution was then sonicated for 2 min using a TPC-15 bath sonicator from Telsonic Ultrasonics, and the solution was quantified using ε = 6550 cm^{-1} M^{-1} ntd^{-1} (25 °C).

Titrations. All fluorescence titrations were conducted at room temperature using prefolded DNA in a "TKE" buffer containing 50 mM Tris-HCl, 150 mM KCl, and 0.5 mM EDTA (pH 7.4 unless indicated otherwise). Fluorescence enhancement and quenching experiments were conducted in Corning 384-well black polystyrene assay plates with nonbinding surfaces (final volume = 70 μL). For each experiment, a 2× solution of APc or DNA (50 nM) was added to the plate followed by 1 volume of DNA or APc solution and mixed once by pipet. Plates were read multiple times to ensure equilibration was reached. Precautions were taken to minimize binding of APcs to plastic tubes and pipet

Table 1: Apparent K_d Values (nM) According to Phthalocyanine Fluorescence Enhancement Titrations

ligand	Htelo	Htelo-mut	Htelo-C	c-kit2	Fl-Htelo	Fl-c-kit2	Fl-c-myc[a]
2	> 1000	> 1000	> 1000	> 1000	> 1000	> 1000	> 1000
3	40 ± 20	> 1000	> 1000	110 ± 8	100 ± 25	74 ± 16	32 ± 24
4	56 ± 6	> 1000	> 1000	132 ± 15	114 ± 41	42 ± 38	54 ± 10
5	70 ± 26	> 1000	> 1000	102 ± 33	118 ± 40	38 ± 31	54 ± 35
6	40 ± 5	> 1000	> 1000	96 ± 40	145 ± 20	62 ± 36	28 ± 10
7	> 1000	> 1000	> 1000	> 1000	> 1000	> 1000	> 1000

[a]Similar results were obtained for unlabeled c-myc DNA.

tips during their handling by making two serial dilutions of each compound in the same series of plastic tubes prior to transferring the 2× solutions into assay plates. After incubation for 1 h, the first dilutions were discarded, and each tube was used for a second, identical serial dilution. This effectively presaturates each tube without increasing the solution concentration of the APc. We have conducted this presaturation up to four times, but the same results were obtained after a single presaturation. For the fluorescence enhancement assays, phthalocyanine fluorescence was monitored by excitation at 630 nm, emission at 705 nm, and using a cutoff filter at 665 nm. For the quenching assays, 5′-fluorescein DNA was excited at 490 nm and emission monitored at 525 nm (cutoff filter = 515 nm). Binding isotherms were analyzed using nonlinear curve fitting of raw binding data to determine half-maximal effective concentrations (EC_{50}) from fluorescence (F) versus total concentration (C). For enhancement experiments, the EC_{50} values were fit using $F = F_{max}(1 - e^{-0.69C/EC_{50}})$. For fluorescence quenching data, the EC_{50} values were fit using $F = (\Delta F_{max-min}e^{-0.69C/EC_{50}}) + F_{min}$. These formulas make no assumptions about binding stoichiometry or ligand depletion. The resulting EC_{50} values were converted into K_d values by assuming identical and independent 2:1 ligand−DNA binding sites according to the formula $K_d = (EC_{50} \times 2) - 12.5$ nM (Tables 1 and 2). Potential differences in binding stoichiometries and cooperativity should impact the calculated values by 3-fold or less. Any 1:1 binding interactions and/or self-association of the phthalocyanines would cause underestimated binding affinities (Tables 1 and 2). These values therefore represent lower limits for binding affinity and upper limits for K_d values.

pH Titrations. APc solutions (2 μM) were prepared in TKE (pH 4.0) buffer and equilibrated at room temperature for 1 h. To adjust the pH of the sample, a TKE (pH 11.5) buffer containing 2 μM APc was used. pH values were obtained by direct measurement of each sample by an Orion 310 pH meter (Thermo Electron Corp.) equipped with a calomel micro pH electrode (Möller AG). Each APc has four potentially distinct ammonium groups, so pK_a values were estimated as equal to the range of pH values exhibiting fractional changes of 12.5−87.5% compared to the total change in absorbance.

Circular Dichroism (CD) Spectroscopy. Htelo DNA (3 μM) was mixed with 0, 1, 2, or 3 equiv of **3** in 600 μL of TKE buffer (pH 7.4), heated at 95 °C for 15 min, and slowly cooled to room temperature over 6 h. CD spectra were recorded on a Jasco-715 spectropolarimeter using a quartz cell and an instrument scanning speed of 50 nm/min with a response time of 1 s.

Fluorescence quantum yields were calculated according to $\Phi = \Phi_R(I/I_R)(OD_R/OD)$, where Φ = quantum yield, R = reference, I = area under curve, and OD = optical density. The reference sample Cy5 was diluted in PBS to optical densities of 0.01−0.02 (620 nm). Sample solutions containing APcs and 0, 1, or 10 equiv of Htelo DNA were prepared in TKE buffer and diluted to optical densities between 0.01 and 0.02 (620 nm). All samples were excited at 620 nm, and fluorescence spectra were collected at emission between 680 and 800 nm using a 665 nm cutoff filter.

Table 2: Apparent K_d Values (nM) According to DNA Fluorescence Quenching Titrations

compd	competitor[a]	Fl-c-myc	Fl-c-kit2	Fl-Htelo	Fl-Htelo-mut
2	none	380 ± 104	> 1000	> 1000	> 1000
2	CT DNA	308 ± 280	> 1000	> 1000	> 1000
2	$tRNA^{mix}$	> 1000	> 1000	> 1000	> 1000
3	none	42 ± 11	72 ± 14	122 ± 7	374 ± 98
3	CT DNA	46 ± 21	40 ± 21	101 ± 90	> 1000
3	$tRNA^{mix}$	76 ± 10	105 ± 77	176 ± 41	> 1000
4	none	42 ± 14	42 ± 11	96 ± 8	414 ± 186
4	CT DNA	46 ± 20	44 ± 13	73 ± 11	> 1000
4	$tRNA^{mix}$	94 ± 46	96 ± 4	122 ± 20	> 1000
5	none	28 ± 6	66 ± 26	126 ± 30	820 ± 291
5	CT DNA	18 ± 1	54 ± 43	88 ± 36	> 1000
5	$tRNA^{mix}$	58 ± 23	68 ± 44	191 ± 57	> 1000
6	none	44 ± 20	36 ± 14	108 ± 30	531 ± 378
6	CT DNA	22 ± 8	63 ± 55	96 ± 16	> 1000
6	$tRNA^{mix}$	88 ± 55	84 ± 77	201 ± 65	> 1000
7	none	> 1000	> 1000	> 1000	> 1000
7	CT DNA	> 1000	> 1000	> 1000	> 1000
7	$tRNA^{mix}$	> 1000	> 1000	> 1000	> 1000

[a]A 1000-fold excess of CT DNA or $tRNA^{mix}$ (nucleotide basis) was included when indicated.

RESULTS

Circular Dichroism (CD) Spectroscopy. The global secondary structure of Htelo DNA was monitored in the presence and absence of compound **3** in 150 mM KCl (pH 7.4) (Figure 2A). The CD spectrum of Htelo DNA in the absence of **3** is consistent with a complex mixture of parallel and mostly antiparallel structures having a strong positive peak centered at 293 nm, a shoulder at 265 nm, and a small negative peak near 238 nm (*33*, *34*). When Htelo DNA was refolded by heating in the presence of 1−3 equiv of compound **3**, a dramatic increase in ellipticity at 265 nm and a decrease at 293 nm were observed (Figure 2A). This transition is consistent with the formation of parallel G-quadruplex structure(s) (*34*−*36*). These CD experiments were conducted at DNA concentrations (3 μM) that were well above the K_d value for this binding interaction (∼0.05 μM). The observed concentration dependence therefore suggests a 2:1 ligand:DNA binding stoichiometry (Figure 2A). Similar 2:1 binding stoichiometries and strong preferences for parallel G-quadruplex structure(s) have also been reported for phthalocyanines containing guanidinium and quarternary ammonium groups (*26*, *28*, *29*). Taken together, these results are consistent with end stacking of

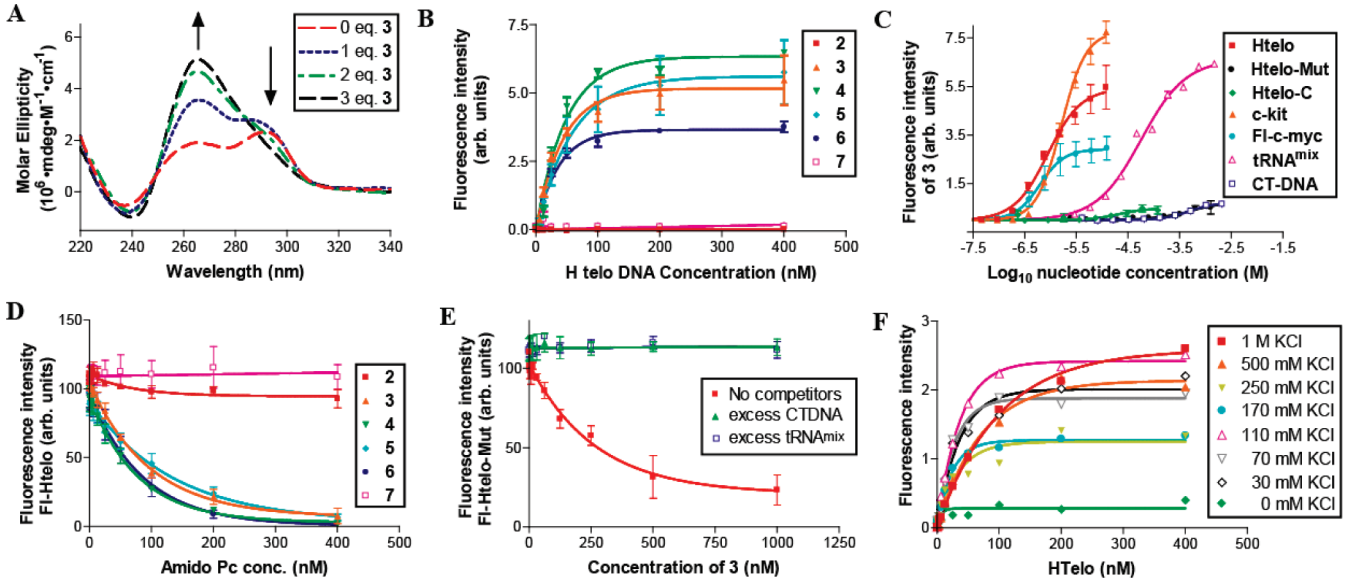

FIGURE 2: (A) CD spectra of 3 μM Htelo upon titration with 0−3 equiv of compound **3**. (B) Fluorescence intensities of 25 nM solutions of **2**−**7** (excitation 630 nm, emission 705 nm) upon titration with Htelo DNA. (C) Fluorescence intensities of 25 nM solutions of **3** upon addition of variable nucleic acids. (D) Fluorescence quenching of 25 nM solutions of Fl-Htelo DNA (excitation 495 nm, emission 520 nm) upon addition of compounds **2**−**7**. (E) Fluorescence quenching of a 25 nM solution of Fl-Htelo-mut (excitation 495 nm, emission 525 nm) upon addition of compound **3** in the presence or absence of a 1000-fold excess (per nucleotide basis) of calf thymus (CT) DNA or a mixture of tRNAs. (F) Fluorescence intensities of 25 nM solutions of compound **3** upon addition of Htelo DNA in the presence of 0−1 M KCl. All samples were prepared and analyzed in a "TKE" buffer containing 50 mM Tris-HCl (pH 7.4) and 0.5 mM EDTA. Titrations shown in (A)−(E) contained 150 mM KCl.

phthalocyanines onto both faces of the "propeller"-type structure of the human telomeric quadruplex (*37*, *38*). This parallel conformation was first observed in high-resolution crystal structures (*37*, *38*) and is the dominant form in solution under conditions of molecular crowding and when bound to quaternary ammonium and guanidino phthalocyanines (*28*−*30*, *34*, *35*). To determine the ability of compound **3** to refold antiparallel G-quadruplex structures at room temperature, the CD spectrum of Htelo DNA (prefolded in 150 mM KCl) was monitored upon addition of compound **3** (2 equiv). No significant changes in the Htelo CD spectrum were observed even after 12 h, suggesting a lack of "chaperone" activity by this compound under these conditions at room temperature (*39*, *40*).

Fluorescence Enhancement Titrations. Amido phthalocyanines **3**−**6** exhibit highly desirable "turn-on" fluorescence upon binding G-quadruplex DNA (*41*−*44*). At pH 7.4, the quantum yields of phthalocyanines **3**−**6** increased by 100−400-fold upon titration of the prefolded "Htelo" DNA: GTTA(GGGTTA)$_4$GG (Figure 2B). Direct comparisons with Cy5 as a fluorescent standard (Φ = 0.27) (*45*) indicated that the quantum yield (Φ) of **3** increased about 400-fold (from $\leq 1.2 \times 10^{-4}$ to $\approx$0.05) upon saturation with Htelo DNA. This modest quantum yield (0.05) is offset by the large molar extinction coefficients (30000−150000 cm^{-1} M^{-1}) exhibited by these compounds. The resulting brightness of the complexes allows very sensitive detection of G-quadruplex binding at probe concentrations as low as 1 nM. In contrast, compounds **2** and **7** exhibited little, if any, fluorescence enhancement upon addition of any of the nucleic acids evaluated at pH 7.4 (Figure 2B). Fluorescence data collected using 25 nM solutions of **3**−**6** were analyzed using an independent 2:1 binding model to reveal equilibrium dissociation constants (K_d) of approximately 50 ± 20 nM (Table 1). These values are very similar to the Htelo binding affinities reported for tetramethylpyridinium porphyrazines and quaternary ammonium zinc phthalocyanines ($K_d \approx 120$ nM) (*27*−*29*), but are 10-fold lower than guanidino phthalocyanines ($K_d \approx 6$ nM) (*26*).

Table 3: C_{50} Values (μM Nucleotides) According to Phthalocyanine Fluorescence Enhancement Titrations

ligand	Htelo	tRNA^{mix}	CT DNA
2	> 30	> 1000	> 1000
3	0.9 ± 0.5	50 ± 2	530 ± 110
4	1.0 ± 0.1	37 ± 3	440 ± 220
5	1.2 ± 0.4	70 ± 2	330 ± 210
6	0.8 ± 0.1	80 ± 4	400 ± 100
7	> 30	> 1000	> 1000

To probe the structure selectivity of APcs, we also evaluated a closely related, but unfolded variant of Htelo DNA, "Htelo-mut", GTTA(GAGTTA)$_4$GG, and the C-rich complement strand of Htelo, "Htelo-C" DNA, CC(TAACCC)$_4$TAAC, that can form an i-motif under acidic conditions (*46*). In stark contrast to Htelo, little or no increase in fluorescence from compounds **3**−**6** was observed upon titration of Htelo-mut or Htelo-C (Figure 2C). To probe the G-quadruplex specificity of APcs **3**−**6** relative to heterogeneous nucleic acids derived from cells, the fluorescence intensities of 25 nM solutions of **2**−**7** were monitored upon titration of a mixture of tRNA or calf thymus (CT) DNA. Highly selective G-quadruplex binding was revealed by comparing these binding isotherms on a log (nucleotide) scale (Figure 2C). This plot compares oligomeric and polymeric nucleic acids of differing lengths and reflects both the number of binding sites and affinities. With the assumption that the size and frequency of binding sites (in nucleotides) are roughly similar, these data indicate that compounds **3**−**6** bind to G-quadruplex DNA with at least 50- and 500-fold higher affinities than tRNA and CT DNA, respectively (Figure 2C and Table 3).

To evaluate the Htelo selectivity of these compounds relative to other G-quadruplex structures, the fluorescence intensities of

2−**7** were monitored upon titration of G-quadruplex sequences derived from the c-kit promoter "c-kit2" that sits −162 to −115 bp upstream of the transcription start site (*47*, *48*) and "c-myc" positioned −141 to −110 upstream of the c-myc P1 promoter (*49*−*51*). Once again, no fluorescence enhancements from **2** or **7** were observed, while **3**−**6** exhibited fluorescence increases of 200−800-fold depending on the G-quadruplex added (Figure 2C). Apparent K_d values ranging from 30 to 150 nM were observed for compounds **3**−**6** and each of the three G-quadruplex structures (Table 1). The small differences in affinities between the fluorescein-labeled G-quadruplexes suggest the following APc−quadruplex selectivity: c-myc > c-kit2 > Htelo. This same trend is also observed using an orthogonal assay that measures fluorescence changes of the DNA upon addition of each APc.

Fluorescence Quenching Titrations. While fluorescence enhancement titrations provide a powerful and direct means to measure binding affinities (*42*, *43*, *52*), the lack of fluorescence enhancement does not necessarily prove the lack of binding. The G-quadruplex affinity and specificity of compounds **2**−**7** were therefore reevaluated by monitoring the fluorescence emissions from 5′-fluorescein end-labeled DNAs upon titration of each compound. This approach has been widely used to study RNA−ligand binding (*53*−*59*) and, more recently, G-quadruplex interactions (*26*). Upon ligand binding, the microenvironment and therefore fluorescence properties of the 5′-fluorescein are altered due to changes in nucleic acid structure, dynamics, or proximity to the bound ligand itself. Unlike FRET-based techniques, spectral overlap is not a prerequisite for useful fluorescent readout as demonstrated by the 6-fold quenching of fluorescein-labeled RNA upon binding aminoglycosides (*53*). Similarly, compounds **3**−**6** caused a dramatic and reversible quenching of fluorescein-labeled nucleic acids (Figure 2D and Table 2). To evaluate the potential impact of fluorescein attachment on the apparent K_d values measured using this method, we conducted fluorescence enhancement experiments (described above) using DNAs carrying either a 5′-OH or 5′-fluorescein (Table 1). In all cases, the variations in apparent K_d values between the labeled and unlabeled DNAs were 3-fold or less, indicating relatively small perturbations by the 5′-fluorescein tag. Consistent with this, CD experiments indicated nearly identical global secondary structures and thermal stabilities of Htelo DNA for molecules with 5′-OH and 5′-fluorescein groups (not shown).

Consistent with the results obtained by fluorescence enhancement experiments, fluorescein-quenching isotherms indicated that compounds **3**−**6** bound to Htelo, c-kit and c-myc quadruplexes with apparent K_d values in the range of 20−130 nM (Table 2). The apparent affinities for the mutant quadruplex "Fl-Htelo-mut" were much lower with values ≥400 nM (Table 2). In contrast, compounds **2** and **7** exhibited little, if any, quenching of fluorescein-labeled DNA (Figure 2D). These data confirm the trends revealed by the fluorescence enhancement titration assays and further illustrate the importance of the variable number of methylene groups in compounds **2**−**5**, as well as the poor quadruplex affinity of compounds **2** and **7**.

One key advantage to using fluorescently labeled DNA for binding experiments is the opportunity to conduct titrations in the presence of a large excess of unlabeled nucleic acids. By comparing the changes in affinity measured in the presence versus absence of competitor nucleic acids, information about the specificity of these binding interactions can be revealed (*52*, *60*). Compounds **3**−**6** exhibited essentially the same apparent K_d values for G-quadruplex binding in the presence and absence of a 1000-fold excess of CT DNA (Table 2). These data confirm the excellent G-quadruplex selectivity of APcs compared to bulk genomic DNA. Approximately 2-fold higher K_d values were observed in the presence of a 1000-fold excess of $tRNA^{mix}$ (Table 2). These results are consistent with the fluorescence enhancement titrations, where compounds **3**−**6** exhibited G-quadruplex affinities that were 50- and 500-fold higher than $tRNA^{mix}$ and CT DNA, respectively (Figure 2C and Table 3). Strictly nonspecific binding interactions between compounds **3**−**6** and Fl-Htelo-mut were revealed by the total inhibition of APc binding by both CT DNA and $tRNA^{mix}$ (Figure 2E and Table 2). Together, these results indicate that structured nucleic acids (quadruplex > tRNA > duplex) exhibit higher APc affinities than poorly structured and unfolded oligonucleotides (Htelo-mut).

Variable Ionic Strength Titrations. We tested the salt dependence of the binding interactions between compound **3** and Htelo DNA over a range of 0−1 M KCl. Interestingly, the apparent affinity remained essentially constant (K_d = 33 ± 7 nM) from 30 to 250 mM KCl (Figure 2F). A similar result was reported for the cationic porphyrin TMPyP4 over this same range of KCl (*61*). Upon raising the KCl concentration to 500 mM the apparent affinity of compound **3** dropped only slightly to K_d = 49 nM, and at 1 M KCl the apparent K_d = 68 nM (Figure 2F). TMPyP4, in contrast, exhibited very weak binding at these high salt concentrations (*61*). In the absence of KCl, no binding of **3** was observed, due to the destabilization and unfolding of Htelo DNA (Figure 2F). These results indicate that electrostatics are not the only energetic driving forces responsible for APc−quadruplex binding. Dispersion and/or π-stacking forces must also contribute to binding and to a greater extent than TMPyP4. As a control experiment, we monitored the UV absorbance spectrum of compound **3** as a function of KCl concentration. From 0 to 500 mM KCl (pH 7.4) no change in the absorbance of compound **3** was observed, suggesting no changes in the aggregation state of **3** over this concentration range. Additional control experiments were conducted to assess possible structural rearrangements of Htelo DNA as a function of KCl. CD experiments conducted using Htelo alone or as a 1:2 mixture with compound **3** indicated little, if any, changes in the CD spectrum of Htelo from 30 to 1000 mM KCl. In contrast, small changes in pH can have a profound impact on both self-association and DNA binding of APcs.

pH-Dependent G-Quadruplex Binding. Initial evidence that pH-dependent phenomena were responsible for the dramatic loss in G-quadruplex binding affinity of compound **2** as compared to **3**−**5** was revealed by the ^{1}H NMR spectra of compounds **2**− **5** (Figure 3). The chemical shifts of the NH_3^+ groups in each compound varied as a function of the number of methylene units separating the ammonium from each carbonyl group of the APc scaffold. The chemical shifts of NH_3^+ were 8.39, 8.03, 7.92, and 7.89 for compounds **2**, **3**, **4**, and **5**, respectively (Figure 3). These data correlate with the predicted pK_a values for the following series of structurally related model compounds: 2-amino-*N*-phenylacetamide (pK_a 7.8), 3-amino-*N*-phenylpropanamide (pK_a 9.0), 4-amino-*N*-phenylbutanamide (pK_a 9.9), and 5-amino-*N*-phenylpentanamide (pK_a 10.6). Values were calculated using Advanced Chemistry Development (ACD/Laboratories) Software V8.14 and obtained from SciFinder Scholar. These values are for the monocation of each model compound and therefore represent the upper limits of expected

pK_a values for the tetracations of **2**−**5**, and are the expected pK_a values for the monocations of **2**−**5**.

To evaluate the pH dependence of quadruplex binding, Htelo DNA was titrated into 25 nM solutions of compounds **2** and **3** under conditions of variable pH (Figure 4A,B). Consistent with titrations conducted at pH 7.4 (Figure 2B), compound **2** exhibited no fluorescence enhancement upon addition of DNA at pH 7.7 and above (Figure 4A). Under slightly acidic conditions (pH < 6.8), however, compound **2** exhibited DNA binding comparable to that of compounds **3**−**5** (Figure 4A). Very similar results were obtained for compound **3** except that higher pH values (pH > 8) were needed to attenuate quadruplex binding (Figure 4B). To evaluate the origin of this effect, the absorbance spectra of 2 μM solutions of compounds **2** and **3** were monitored as a function of pH (Figure 4C−E). Under slightly acidic conditions, both compounds were fully soluble and exhibited strong absorbance peaks at 635 nm indicative of common "H-type" (face-to-face) dimers/multimers (*62*). As the pH of each solution increased from 4 to 10, changes consistent with the formation of extended "J-type" (side-by-side) aggregates were revealed by the emergence of an absorbance peak at 720 nm and the formation of colloidal suspensions in solution (*62*). According to their absorbance spectra, compounds **3**−**7** are primarily H-type dimers/multimers available for DNA binding at pH 7.4 and below (similar to Figure 4C, pH = 4.0). In the absence of DNA, J-aggregates were apparent for compound **2** at pH ≥6.8 (Figure 4C) while pH values ≥8.0 were needed before any J-aggregates were observed for compound **3**. These values correlate with the pH-dependent fluorescence changes of each compound upon addition of Htelo DNA (Figure 4A,B) and indicate that J-type, highly aggregated APcs are incapable of DNA binding.

By plotting pH versus absorbance at 635 nm, we estimated that the ammonium groups in compound **2** have pK_a values ranging from 6.4 to 7.2 (Figure 4F), while the pK_a values for compound **3** are 7.3−8.7. These values are for the conversion of soluble face-to-face H-type dimers/multimers into J-aggregates and therefore must be interpreted cautiously. Despite this potential complication, the average difference in apparent pK_a values between **2** and **3** (1.2 units) matches the 1.2 unit difference in pK_a values

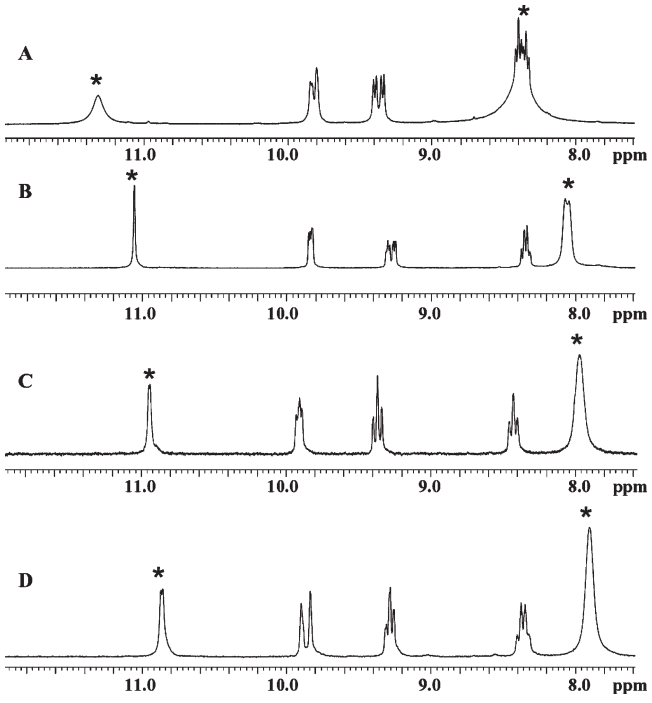

FIGURE 3: Partial ^{1}H NMR spectra of **2**−**5** in DMSO-d_6: (A) **2**, (B) **3**, (C) **4**, and (D) **5**. Protons exhibiting exchange with MeOD-d_3 are indicated with an asterisk.

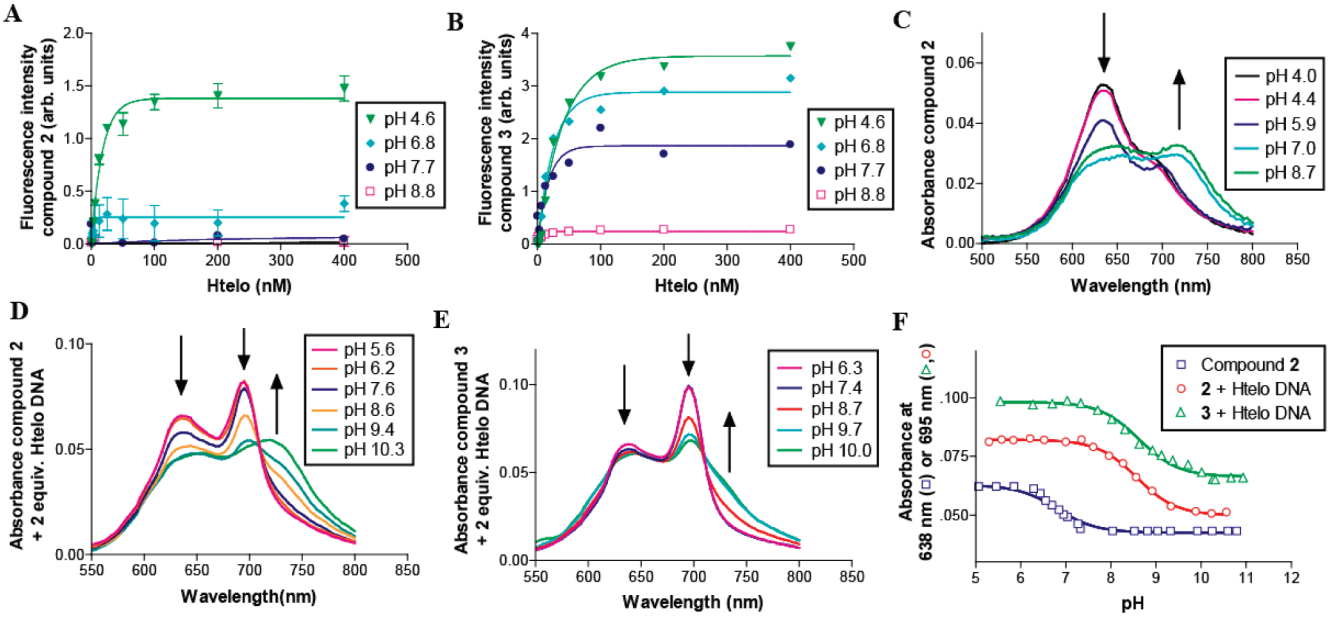

FIGURE 4: (A) Fluorescence intensities of 25 nM solutions of compound **2** (excitation 630 nm, emission 705 nm) upon titration of Htelo DNA under conditions of variable pH. (B) Fluorescence intensities of 25 nM solutions of compound **3** (excitation 630 nm, emission 705 nm) upon titration of Htelo DNA under conditions of variable pH. (C) Absorbance spectra of 2 μM solutions of compound **2** under conditions of variable pH. (D) Absorbance spectra of 2 μM solutions of compound **2** in the presence of 2 equiv of Htelo DNA under conditions of variable pH. (E) Absorbance spectra of 2 μM solutions of compound **3** in the presence of 2 equiv of Htelo DNA under conditions of variable pH. (F) Absorbance of compound **2** or **3** in the presence or absence of 2 equiv of Htelo DNA as a function of pH. All samples were prepared and analyzed in a "TKE" buffer containing 50 mM Tris-HCl, 150 mM KCl, and 0.5 mM EDTA. Arrows shown in (C)−(E) indicate changes in absorbance spectra as the pH is increased from 4 to 10.

predicted for the model compounds 2-amino-*N*-phenylacetamide (pK_a 7.8) and 3-amino-*N*-phenylpropanamide (pK_a 9.0).

The formation of H-type multimers and J-type aggregates, observed at 635 and 720 nm, respectively (*62*), is suppressed by adding a 2-fold excess of Htelo DNA to each sample before basification. The disappearance of these peaks and the emergence of a strong absorbance peak at 695 nm indicate the presence of monomeric phthalocyanines (Figure 4C−E) (*63*). In the presence of 2 equiv of Htelo DNA, the apparent pK_a values for compounds **2** and **3** are quite similar. By using plots of pH versus absorbance at 695 nm, we estimated pK_a values ranging between 7.7−9.0 and 7.9−9.9 for compounds **2** and **3**, respectively, when bound to Htelo DNA (Figure 4F). According to the changes in absorbance of compound **2** at 720 nm upon basification, the minimal pH where "J"-type aggregation can be observed is shifted by approximately +1.3 pH units as compared to the samples lacking DNA (Figure 4C,D). This is consistent with the increased pK_a values measured for compound **2** in the presence versus absence of Htelo DNA and indicates a direct competition between aggregation and DNA binding that is shifted by pH.

DISCUSSION

G-quadruplex structures exhibit a wide variety of folding topologies and loop structures (*7*−*10*). The human telomeric repeat sequence, for example, can exist as a complex mixture of structures in potassium-containing solutions (*33*, *34*, *64*). The parallel "propeller" conformation of Htelo that was first observed in high-resolution crystal structures (*37*, *38*) is the dominant form in solution under conditions of molecular crowding and when bound to quaternary ammonium and guanidino phthalocyanines (*28*−*30*, *34*, *35*, *65*). According to our results, APcs induce formation of the Htelo propeller structure at elevated temperatures, and the resulting 2:1 complexes contain nonaggregated, fluorescent APcs with quantum yields of approximately 0.05.

The binding affinity and specificity of APcs were determined using two direct and complementary fluorescence-based assays by mixing the ligands with prefolded DNA at room temperature. APcs bound to G-quadruplex structures with 100−1000 times higher affinity than duplex and single-stranded nucleic acids. The formation of specific contacts between the ammonium groups of these compounds and quadruplex phosphates is, however, unlikely given the nearly identical G-quadruplex affinity and specificity of compounds **3**−**6** (Tables 1 and 2). The apparent G-quadruplex affinities of compounds **3**−**6** ($K_d \approx 20-200$ nM) were very similar to those reported for quaternary ammonium zinc phthalocyanines and tetramethylpyridinium porphyrazines (*27*−*29*). Taken together, these results strongly suggest that the phthalocyanine scaffold and not the exact identities of the cationic side chains are responsible for the impressive G-quadruplex affinity and specificity of these compounds. Energetically important interactions mediated by APc ammonium groups are likely dominated by two factors, the first being long-range ($1/r$) electrostatic interactions with quadruplex phosphates; the second effect is destabilization of phthalocyanine multimerization via electrostatic repulsion.

Binding reactions that are driven mostly by electrostatic interactions exhibit K_d values that are highly sensitive to the ionic strength of the solution (*66*). The apparent binding affinities of RNA−aminoglycoside interactions, for example, can decrease 1000-fold when binding reactions are conducted under physiological conditions as compared to nearly salt-free solutions (*67*−*69*). In contrast, the apparent Htelo affinity of compound **3** decreased only by a factor of 2 in solutions containing 30 mM KCl as compared to 1 M KCl (Figure 2F). In 0 mM KCl, on the other hand, no binding was observed due to the unfolding of the quadruplex (Figure 2F). Taken together, these results are consistent with the formation of structure-specific base-stacking interactions stabilized by dispersion and/or π-stacking. The expected loss in APc−quadruplex electrostatic binding energy in 1 M KCl is likely compensated by increased stability of shape-selective stacking interactions. These forces are not strong enough, however, to overcome the charge repulsion between G-quadruplex phosphates and compound **7** that exhibited no observable quadruplex binding.

Like guanosine itself, porphyrins, phthalocyanines, and perlyene-based derivatives exhibit a strong tendency to self-associate in aqueous solution. Interestingly, perlyene diimides that were aggregated had improved G-quadruplex specificity as compared to nonaggregated species (*70*). In our case, however, the suppressed pK_a values for the ammonium groups of compound **2** caused formation of high molecular weight "J"-type aggregates at pH ≥6.8 that did not bind to G-quadruplex DNA. By increasing the number of methylene units in this compound, the pK_a values of the ammonium groups increased and the tendency to form J-type aggregates decreased. The soluble, H-type dimers/multimers of compounds **3**−**6** at pH 7.4 are nonfluorescent but capable of binding DNA to generate fluorescent complexes containing monomeric APcs.

Compounds **2**−**6** exhibit pH-dependent self-association that can inhibit G-quadruplex binding. The critical pH value above which self-association becomes dominant is dictated by the pK_a value for the terminal ammonium groups of each compound. The apparent quadruplex affinities measured for these compounds at pH 7.4 (Tables 1 and 2) do not take into account the energetic penalties for dissociation of the soluble H-type multimers. Binding affinities might therefore be enhanced by the synthesis of phthalocyanine derivatives that do not exhibit self-assembly in neutral aqueous solutions. Such compounds, however, might have lower quadruplex specificity (*70*) and will probably not exhibit "turn-on" fluorescence upon binding G-quadruplex DNA because the quantum yields of monomeric zinc and silicon phthalocyanines in water are approximately 0.25 (*71*−*73*), while the quantum yields for quadruplex−APc complexes are about 0.05. This suggests a trade-off between the potential applications of phthalocyanines as fluorescent probes versus drug candidates, where "turn-on" fluorescence is a highly desirable property that facilitates direct DNA binding assays and cellular uptake experiments (*26*, *41*−*44*), and monomeric derivatives exhibit enhanced affinity but diminished fluorescence upon G-quadruplex binding.

In summary, we have reported a new family of G-quadruplex ligands with excellent G-quadruplex affinity and specificity. Through systematic variation of an amido phthalocyanine scaffold, our results showed how electrostatic and stacking interactions can play a complex role in mediating both phthalocyanine aggregation and DNA binding. These results should help future efforts toward the rational design of optimized G-quadruplex-specific fluorescent probes and drug candidates.

REFERENCES

1. Dervan, P. B., Doss, R. M., and Marques, M. A. (2005) Programmable DNA binding oligomers for control of transcription. *Curr. Med. Chem. Anticancer Agents 5*, 373–387.

2. Blackburn, G. M., Gait, M. J., Loakes, D., and Williams, D. (2006) Nucleic Acids in Chemistry and Biology, 3rd ed. The Royal Society of Chemistry, Cambridge.
3. Chaires, J. B., and Mergny, J. L. (2008) Targeting DNA. *Biochimie 90*, 973–975.
4. Dervan, P. B. (2001) Molecular recognition of DNA by small molecules. *Bioorg. Med. Chem. 9*, 2215–2235.
5. Best, T. P., Edelson, B. S., Nickols, N. G., and Dervan, P. B. (2003) Nuclear localization of pyrrole-imidazole polyamide-fluorescein conjugates in cell culture. *Proc. Natl. Acad. Sci. U.S.A. 100*, 12063–12068.
6. Jaaskelainen, I., and Urtti, A. (2002) Cell membranes as barriers for the use of antisense therapeutic agents. *Mini. Rev. Med. Chem. 2*, 307–318.
7. Patel, D. J., Phan, A. T., and Kuryavyi, V. (2007) Human telomere, oncogenic promoter and 5′-UTR G-quadruplexes: diverse higher order DNA and RNA targets for cancer therapeutics. *Nucleic Acids Res. 35*, 7429–7455.
8. Neidle, S., and Parkinson, G. N. (2008) Quadruplex DNA crystal structures and drug design. *Biochimie 90*, 1184–1196.
9. Davis, J. T. (2004) G-quartets 40 years later: from 5′-GMP to molecular biology and supramolecular chemistry. *Angew. Chem., Int. Ed. 43*, 668–698.
10. Burge, S., Parkinson, G. N., Hazel, P., Todd, A. K., and Neidle, S. (2006) Quadruplex DNA: sequence, topology and structure. *Nucleic Acids Res. 34*, 5402–5415.
11. Lane, A. N., Chaires, J. B., Gray, R. D., and Trent, J. O. (2008) Stability and kinetics of G-quadruplex structures. *Nucleic Acids Res. 36*, 5482–5515.
12. Mergny, J. L., Riou, J. F., Mailliet, P., Teulade-Fichou, M. P., and Gilson, E. (2002) Natural and pharmacological regulation of telomerase. *Nucleic Acids Res. 30*, 839–865.
13. Balasubramanian, S., and Neidle, S. (2009) G-quadruplex nucleic acids as therapeutic targets. *Curr. Opin. Chem. Biol. 13*, 345–353.
14. Huppert, J. L., and Balasubramanian, S. (2005) Prevalence of quadruplexes in the human genome. *Nucleic Acids Res. 33*, 2908–2916.
15. Todd, A. K., Johnston, M., and Neidle, S. (2005) Highly prevalent putative quadruplex sequence motifs in human DNA. *Nucleic Acids Res. 33*, 2901–2907.
16. Zhang, R., Lin, Y., and Zhang, C. T. (2008) Greglist: a database listing potential G-quadruplex regulated genes. *Nucleic Acids Res. 36*, D372–376.
17. Hershman, S. G., Chen, Q., Lee, J. Y., Kozak, M. L., Yue, P., Wang, L. S., and Johnson, F. B. (2008) Genomic distribution and functional analyses of potential G-quadruplex-forming sequences in *Saccharomyces cerevisiae*. *Nucleic Acids Res. 36*, 144–156.
18. Rawal, P., Kummarasetti, V. B. R., Ravindran, J., Kumar, N., Halder, K., Sharma, R., Mukerji, M., Das, S. K., and Chowdhury, S. (2006) Genome-wide prediction of G4 DNA as regulatory motifs: role in *Escherichia coli* global regulation. *Genome Res. 16*, 644–655.
19. Luedtke, N. W. (2009) Targeting G-quadruplex DNA with small molecules. *Chimia 63*, 134–139.
20. Monchaud, D., and Teulade-Fichou, M. P. (2008) A hitchhiker's guide to G-quadruplex ligands. *Org. Biomol. Chem. 6*, 627–636.
21. Ou, T. M., Lu, Y. J., Tan, J. H., Huang, Z. S., Wong, K. Y., and Gu, L. Q. (2008) G-quadruplexes: targets in anticancer drug design. *ChemMedChem 3*, 690–713.
22. White, E. W., Tanious, F., Ismail, M. A., Reszka, A. P., Neidle, S., Boykin, D. W., and Wilson, W. D. (2007) Structure-specific recognition of quadruplex DNA by organic cations: influence of shape, substituents and charge. *Biophys. Chem. 126*, 140–153.
23. Phan, A. T., Kuryavyi, V., Gaw, H. Y., and Patel, D. J. (2005) Small-molecule interaction with a five-guanine-tract G-quadruplex structure from the human MYC promoter. *Nat. Chem. Biol. 1*, 167–173.
24. Campbell, N. H., Patel, M., Tofa, A. B., Ghosh, R., Parkinson, G. N., and Neidle, S. (2009) Selectivity in ligand recognition of G-quadruplex loops. *Biochemistry 48*, 1675–1680.
25. Hounsou, C., Guittat, L., Monchaud, D., Jourdan, M., Saettel, N., Mergny, J. L., and Teulade-Fichou, M. P. (2007) G-quadruplex recognition by quinacridines: a SAR, NMR, and biological study. *ChemMedChem 2*, 655–666.
26. Alzeer, J., Vummidi, B. R., Roth, P. J. C., and Luedtke, N. W. (2009) Guanidinium-modified phthalocyanines as high affinity G-quadruplex fluorescent probes and transcriptional regulators. *Angew. Chem., Int. Ed. 48*, 9362–9365.
27. Goncalves, D. P. N., Rodriguez, R., Balasubramanian, S., and Sanders, J. K. M. (2006) Tetramethylpyridiniumporphyrazines—a new class of G-quadruplex inducing and stabilising ligands. *Chem. Commun.,* 4685–4687.
28. Zhang, L., Huang, J., Ren, L., Bai, M., Wu, L., Zhai, B., and Zhou, X. (2008) Synthesis and evaluation of cationic phthalocyanine derivatives as potential inhibitors of telomerase. *Bioorg. Med. Chem. 16*, 303–312.
29. Ren, L. G., Zhang, A. M., Huang, J., Wang, P., Weng, X. C., Zhang, L. X., Liang, F., Tan, Z., and Zhou, X. (2007) Quaternary ammonium zinc phthalocyanine: inhibiting telomerase by stabilizing G quadruplexes and inducing G-quadruplex structure transition and formation. *ChemBioChem 8*, 775–780.
30. Paramasiva, M., Membrin, A., Cogo, S., Alzeer, J., Luedtke, N. W., and Xodo, L. E. (2010) Cellular uptake and binding of guanidine-modified phthalocyanines to KRAS/HRAS G-quadruplexes. *Chem. Commun.,* 625–627.
31. Alzeer, J., Roth, P. J. C., and Luedtke, N. W. (2009) An efficient two-step synthesis of metal-free phthalocyanines using a Zn(II) template. *Chem. Commun.,* 1970–1971.
32. Cong, F.-D., Ning, B., Du, X.-G., Ma, C.-Y., Yu, H.-F., and Chen, B. (2005) Facile synthesis, characterization and property comparisons of tetraaminometallophthylocyanines with and without intramolecular hydrogen bonds. *Dyes Pigm. 66*, 149–154.
33. Kypr, J., Kejnovska, I., Renciuk, D., and Vorlickova, M. (2009) Circular dichroism and conformational polymorphism of DNA. *Nucleic Acids Res. 37*, 1713–1725.
34. Xue, Y., Kan, Z. Y., Wang, Q., Yao, Y., Liu, J., Hao, Y. H., and Tan, Z. (2007) Human telomeric DNA forms parallel-stranded intramolecular G-quadruplex in K^+ solution under molecular crowding condition. *J. Am. Chem. Soc. 129*, 11185–11191.
35. Balagurumoorthy, P., Brahmachari, S. K., Mohanty, D., Bansal, M., and Sasisekharan, V. (1992) Hairpin and parallel quartet structures for telomeric sequences. *Nucleic Acids Res. 20*, 4061–4067.
36. Garner, T. P., Williams, H. E., Gluszyk, K. I., Roe, S., Oldham, N. J., Stevens, M. F., Moses, J. E., and Searle, M. S. (2009) Selectivity of small molecule ligands for parallel and anti-parallel DNA G-quadruplex structures. *Org. Biomol. Chem. 7*, 4194–4200.
37. Parkinson, G. N., Ghosh, R., and Neidle, S. (2007) Structural basis for binding of porphyrin to human telomeres. *Biochemistry 46*, 2390–2397.
38. Parkinson, G. N., Lee, M. P., and Neidle, S. (2002) Crystal structure of parallel quadruplexes from human telomeric DNA. *Nature 417*, 876–880.
39. De Cian, A., and Mergny, J. L. (2007) Quadruplex ligands may act as molecular chaperones for tetramolecular quadruplex formation. *Nucleic Acids Res. 35*, 2483–2493.
40. Rodriguez, R., Pantos, G. D., Goncalves, D. P., Sanders, J. K., and Balasubramanian, S. (2007) Ligand-driven G-quadruplex conformational switching by using an unusual mode of interaction. *Angew. Chem., Int. Ed. 46*, 5405–5407.
41. Arthanari, H., Basu, S., Kawano, T. L., and Bolton, P. H. (1998) Fluorescent dyes specific for quadruplex DNA. *Nucleic Acids Res. 26*, 3724–3728.
42. Koeppel, F., Riou, J. F., Laoui, A., Mailliet, P., Arimondo, P. B., Labit, D., Petitgenet, O., Helene, C., and Mergny, J. L. (2001) Ethidium derivatives bind to G-quartets, inhibit telomerase and act as fluorescent probes for quadruplexes. *Nucleic Acids Res. 29*, 1087–1096.
43. Yang, P., De Cian, A., Teulade-Fichou, M. P., Mergny, J. L., and Monchaud, D. (2009) Engineering bisquinolinium/thiazole orange conjugates for fluorescent sensing of G-quadruplex DNA. *Angew. Chem., Int. Ed. 48*, 2188–2191.
44. Ma, D. L., Che, C. M., and Yan, S. C. (2009) Platinum(II) complexes with dipyridophenazine ligands as human telomerase inhibitors and luminescent probes for G-quadruplex DNA. *J. Am. Chem. Soc. 131*, 1835–1846.
45. Mujumdar, S. R., Mujumdar, R. B., Grant, C. M., and Waggoner, A. S. (1996) Cyanine-labeling reagents: sulfobenzindocyanine succinimidyl esters. *Bioconjugate Chem. 7*, 356–362.
46. Phan, A. T., and Mergny, J. L. (2002) Human telomeric DNA: G-quadruplex, i-motif and Watson-Crick double helix. *Nucleic Acids Res. 30*, 4618–4625.
47. Fernando, H., Reszka, A. P., Huppert, J., Ladame, S., Rankin, S., Venkitaraman, A. R., Neidle, S., and Balasubramanian, S. (2006) A conserved quadruplex motif located in a transcription activation site of the human c-kit oncogene. *Biochemistry 45*, 7854–7860.
48. Hsu, S. T., Varnai, P., Bugaut, A., Reszka, A. P., Neidle, S., and Balasubramanian, S. (2009) A G-rich sequence within the c-kit oncogene promoter forms a parallel G-quadruplex having asymmetric G-tetrad dynamics. *J. Am. Chem. Soc. 131*, 13399–13409.
49. Boles, T. C., and Hogan, M. E. (1987) DNA structure equilibria in the human c-myc gene. *Biochemistry 26*, 367–376.
50. Simonsson, T., Pecinka, P., and Kubista, M. (1998) DNA tetraplex formation in the control region of c-myc. *Nucleic Acids Res. 26*, 1167–1172.

51. Ambrus, A., Chen, D., Dai, J., Jones, R. A., and Yang, D. (2005) Solution structure of the biologically relevant G-quadruplex element in the human c-MYC promoter. Implications for G-quadruplex stabilization. *Biochemistry 44*, 2048–2058.
52. Luedtke, N. W., and Tor, Y. (2003) Fluorescence-based methods for evaluating the RNA affinity and specificity of HIV-1 Rev-RRE inhibitors. *Biopolymers 70*, 103–119.
53. Llano-Sotelo, B., and Chow, C. S. (1999) RNA-aminoglycoside antibiotic interactions: fluorescence detection of binding and conformational change. *Bioorg. Med. Chem. Lett. 9*, 213–216.
54. Denap, J. C., Thomas, J. R., Musk, D. J., and Hergenrother, P. J. (2004) Combating drug-resistant bacteria: small molecule mimics of plasmid incompatibility as antiplasmid compounds. *J. Am. Chem. Soc. 126*, 15402–15404.
55. Thomas, J. R., DeNap, J. C., Wong, M. L., and Hergenrother, P. J. (2005) The relationship between aminoglycosides' RNA binding proclivity and their antiplasmid effect on an IncB plasmid. *Biochemistry 44*, 6800–6808.
56. Haddad, J., Kotra, L. P., Llano-Sotelo, B., Kim, C., Azucena, E. F., Jr., Liu, M., Vakulenko, S. B., Chow, C. S., and Mobashery, S. (2002) Design of novel antibiotics that bind to the ribosomal acyltransfer site. *J. Am. Chem. Soc. 124*, 3229–3237.
57. Liu, X., Thomas, J. R., and Hergenrother, P. J. (2004) Deoxystreptamine dimers bind to RNA hairpin loops. *J. Am. Chem. Soc. 126*, 9196–9197.
58. Tok, J. B., Bi, L., and Saenz, M. (2005) Specific recognition of napthyridine-based ligands toward guanine-containing bulges in RNA duplexes and RNA-DNA heteroduplexes. *Bioorg. Med. Chem. Lett. 15*, 827–831.
59. Thomas, J. R., Liu, X., and Hergenrother, P. J. (2006) Biochemical and thermodynamic characterization of compounds that bind to RNA hairpin loops: toward an understanding of selectivity. *Biochemistry 45*, 10928–10938.
60. Thomas, J. R., and Hergenrother, P. J. (2008) Targeting RNA with small molecules. *Chem. Rev. 108*, 1171–1224.
61. Freyer, M. W., Buscaglia, R., Kaplan, K., Cashman, D., Hurley, L. H., and Lewis, E. A. (2007) Biophysical studies of the c-MYC NHE III1 promoter: model quadruplex interactions with a cationic porphyrin. *Biophys. J. 92*, 2007–2015.
62. Snow, A. W. (2003) Phthalocyanine: properties and materials, in The Porphyrin Handbook (Kadish, K. M., Smith, K. M., and Guilard, R., Eds.) Vol. *17*, Elsevier Science, Amsterdam.
63. de Oliveira, K. T., de Assis, F. F., Ribeiro, A. O., Neri, C. R., Fernandes, A. U., Baptista, M. S., Lopes, N. P., Serra, O. A., and Iamamoto, Y. (2009) Synthesis of phthalocyanines-ALA conjugates: water-soluble compounds with low aggregation. *J. Org. Chem. 74*, 7962–7965.
64. Li, J., Correia, J. J., Wang, L., Trent, J. O., and Chaires, J. B. (2005) Not so crystal clear: the structure of the human telomere G-quadruplex in solution differs from that present in a crystal. *Nucleic Acids Res. 33*, 4649–4659.
65. Miyoshi, D., Matsumura, S., Nakano, S., and Sugimoto, N. (2004) Duplex dissociation of telomere DNAs induced by molecular crowding. *J. Am. Chem. Soc. 126*, 165–169.
66. Garcia-Garcia, C., and Draper, D. E. (2003) Electrostatic interactions in a peptide−RNA complex. *J. Mol. Biol. 331*, 75–88.
67. Cowan, J. A., Ohyama, T., Wang, D., and Natarajan, K. (2000) Recognition of a cognate RNA aptamer by neomycin B: quantitative evaluation of hydrogen bonding and electrostatic interactions. *Nucleic Acids Res. 28*, 2935–2942.
68. Michael, K., Wang, H., and Tor, Y. (1999) Enhanced RNA binding of dimerized aminoglycosides. *Bioorg. Med. Chem. 7*, 1361–1371.
69. Marin, I., Abad, J. P., Urena, D., and Amils, R. (1995) High-ionic strength interference of ribosomal inhibition produced by aminoglycoside antibiotics. *Biochemistry 34*, 16519–16523.
70. Kern, J. T., Thomas, P. W., and Kerwin, S. M. (2002) The relationship between ligand aggregation and G-quadruplex DNA selectivity in a series of 3,4,9,10-perylenetetracarboxylic acid diimides. *Biochemistry 41*, 11379–11389.
71. Cormick, M. P., Rovera, M., and Durantini, E. N. (2008) Synthesis, spectroscopic properties and photodynamic activity of a novel Zn(II) phthalocyanine substituted by fluconazole groups. *J. Photochem. Photobiol., A 194*, 220–229.
72. Negri, R. M., Zalts, A., Román, E. A., Aramendía, P. F., and Braslavsky, S. E. (1991) Carboxylated zinc phthalocyanine influence of dimerization on the spectroscopic properties. *Photochem. Photobiol. 53*, 317–322.
73. Zhu, Y.-J., Huang, J.-D., Jiang, X.-J., and Sun, J.-C. (2006) Novel silicon phthalocyanines axially modified by morpholine. *Inorg. Chem. Commun. 9*, 473–477.